

Review

# Finite Reynolds Number Effect on Small-Scale Statistics of Homogeneous Isotropic Turbulence

S. L. Tang <sup>1,\*</sup> , L. Danaila <sup>2</sup> and R. A. Antonia <sup>3</sup><sup>1</sup> Center for Turbulence Control, Harbin Institute of Technology, Shenzhen 518055, China<sup>2</sup> Normandie University, UNIROUEN, UNICAEN, CNRS, M2C, 76000 Rouen, France; luminita.danaila@univ-rouen.fr<sup>3</sup> School of Engineering, University of Newcastle, Newcastle 2308, Australia; robert.antonio@newcastle.edu.au

\* Correspondence: shunlin.tang88@gmail.com

**Abstract:** Since about 1997, the realisation that the finite Reynolds number (FRN) effect needs to be carefully taken into account when assessing the behaviour of small-scale statistics came to the fore. The FRN effect can be analysed either in the real domain or in the spectral domain via the scale-by-scale energy budget equation or the transport equation for the energy spectrum. This analysis indicates that the inertial range (IR) is established only when the Taylor microscale Reynolds number  $Re_\lambda$  is infinitely large, thus raising doubts about published power-law exponents at finite values of  $Re_\lambda$ , for either the second-order velocity structure function  $\overline{(\delta u)^2}$  or the energy spectrum. Here, we focus on the transport equation of  $\overline{(\delta u)^2}$  in decaying grid turbulence, which represents a close approximation to homogeneous isotropic turbulence. Regarding small-scale effects, the large-scale forcing term associated with streamwise advection decreases as  $Re_\lambda$  increases and finally disappears when  $Re_\lambda$  is sufficiently large. An approach based on the dual scaling of  $\overline{(\delta u)^2}$ , i.e., a scaling based on the Kolmogorov scales (when the separation  $r$  is small) and another based on the integral scales (when  $r$  is large), yields  $\overline{(\delta u)^2} \sim r^{2/3}$  when  $Re_\lambda$  is infinitely large. This approach also yields  $\overline{(\delta u)^n} \sim r^{n/3}$  when  $Re_\lambda$  is infinitely large. These results seem to be supported by the trend as  $Re_\lambda$  increases according to the available experimental data. Overall, the results for decaying turbulence strongly suggest that a tendency towards the predictions of K41 cannot be dismissed at least at Reynolds numbers that are currently beyond the reach of experiments and direct numerical simulations.

**Keywords:** homogeneous isotropic turbulence; small-scale statistics; finite Reynolds number effect



**Citation:** Tang, S.L.; Danaila, L.; Antonia, R.A. Finite Reynolds Number Effect on Small-Scale Statistics of Homogeneous Isotropic Turbulence. *Atmosphere* **2024**, *15*, 540. <https://doi.org/10.3390/atmos15050540>

Academic Editors: Annick Pouquet and David McComb

Received: 29 February 2024

Revised: 8 April 2024

Accepted: 26 April 2024

Published: 28 April 2024



**Copyright:** © 2024 by the authors. Licensee MDPI, Basel, Switzerland. This article is an open access article distributed under the terms and conditions of the Creative Commons Attribution (CC BY) license (<https://creativecommons.org/licenses/by/4.0/>).

## 1. Introduction

The study of small-scale turbulence is of significant theoretical and practical interest (see the review by Sreenivasan and Antonia [1]). As an example, an improved knowledge of the small-scale motion can lead to an improvement in turbulence models, e.g., the  $k - \epsilon$  model and large eddy simulations via the subgrid scale model. Since the review by Sreenivasan and Antonia [1], significant research has been carried out on the effect of the Reynolds number on small-scale statistics. The earliest research was by Qian [2,3] who introduced the term finite Reynolds number (FRN) effect. This effect is best investigated using either the Kármán–Howarth [4] or generalized Kolmogorov equation in a physical space [5] and spectral space, which is Lin’s equation [6]. The framework provided by these equations allows the constraints imposed on inertial range scales by both the large scales and the dissipative scales to be readily assessed in the context of the FRN effect. This aspect constitutes one objective of the present review.

Starting with the Kármán–Howarth (KH) equation [4], which the authors described as the fundamental equation for the propagation of the two-point velocity correlation function

in homogeneous isotropic turbulence (HIT), Kolmogorov [7] obtained the following relation between  $\overline{(\delta u)^2}$  and  $\overline{(\delta u)^3}$ , the second- and third-order velocity structure functions

$$\overline{(\delta u)^3} = 6\nu \frac{\partial}{\partial r} \overline{(\delta u)^2} - \frac{4}{5} \bar{\epsilon} r, \tag{1}$$

where  $u$  is the longitudinal velocity fluctuation in the direction  $x$ ,  $\delta u = u(x+r) - u(x)$ ,  $r$  being the separation in the direction  $x$ ; the overbar denotes time averaging;  $\bar{\epsilon}$  is the mean dissipation rate of the turbulent kinetic energy; and  $\nu$  is the fluid kinematic viscosity. To arrive at (1), the non-stationary ( $\partial/\partial t$ ) term in the KH equation was neglected. With the further assumption that viscosity is not important in a range identified with the inertial range (IR), where  $\eta \ll r \ll L$  ( $\eta = (\nu^3/\bar{\epsilon})^{1/4}$  is the Kolmogorov length scale and  $L$  is the integral length scale), (1) reduces to

$$\overline{(\delta u)^3} = -\frac{4}{5} \bar{\epsilon} r, \tag{2}$$

a relation that is generally referred to as the 4/5 law. As pointed out by McComb [8], the use of the prefactor in naming this law is unusual since most laws are named after the exponent of  $r$ . It does however highlight the fact that it is the only law, at least in the context of HIT, where the prefactor is known exactly. The derivation of (1) has been the subject of much scrutiny, e.g., [9–14]. Yaglom [15] noted that Kolmogorov’s proof of (1) is not rigorous since the KH equation is valid for fully (global) homogeneous and isotropic turbulence, whereas Kolmogorov’s physical arguments imply only local homogeneity and local isotropy at large Reynolds numbers. In Hill’s [13] proof, (1) holds for a locally homogeneous and isotropic velocity field that satisfies the N-S equation and incompressibility. Hill [13] also obtained (2) without using the incompressibility conditions on the second- and third-order structure functions.

It is worth emphasizing that (2) is an asymptotic result, valid only when  $Re_\lambda (= u' \lambda / \nu$ , where  $\lambda = u' / (\partial u / \partial x)'$  is the Taylor microscale and a prime denotes an r.m.s value) is very large. It is evident that the issue of how (2) is approached as  $Re_\lambda$  increases cannot be tackled with the use of (1) since the latter ignores the effect of the large scales on the small scales. To tackle this issue correctly, the non-stationarity needs to be reinstated in (1), as advocated for example by Danaïla et al. [5], allowing the behaviour of the small scales to be assessed correctly at a finite value of  $Re_\lambda$ . Equivalently, one could use the KH equation (in physical space) or Lin’s equation (in spectral space) [6] (see also [16]). It is appropriate to highlight the work of Qian [2,3], which has paved the way towards a clearer understanding of the finite Reynolds number (FRN) effect. Kolmogorov [17] predicted that, in the IR, the  $n^{th}$ -order velocity structure function is given, after normalizing according to the Kolmogorov scales, by

$$\frac{\overline{(\delta u)^n}}{u_K^n} = A_n \left( \frac{r}{\eta} \right)^{n/3}, \tag{3}$$

where  $A_n$  are universal constants and  $u_K (= (\nu \bar{\epsilon})^{1/4})$  is the Kolmogorov velocity scale. Since about 1997, significant evidence, e.g., [2,3,18–32], has accumulated indicating that particular attention needs to be paid to the FRN effect when assessing the scaling behaviour of the velocity structure functions. These studies indicate that (2) and, more generally, the  $n$ -thirds law in (3) are in fact approached very slowly; thus, a very large value of  $Re_\lambda$  may be required before the IR is unambiguously established. It is worth mentioning that, in order to achieve relatively large values of  $Re_\lambda$  in laboratory experiments, several strategies have been used by the experimentalist such as the use of an active grid, e.g., [33–35] or low temperature helium gas [20], or by varying the density of the fluid, e.g., [36–40]. Kolmogorov [41] or K62 (see also Oboukhov [42]) made an important modification to (3),

which has been widely interpreted as the effect of the spatio-temporal intermittency of  $\epsilon$  [1]. (3) was replaced by

$$\frac{\overline{(\delta u)^n}}{u'^n} \sim \left(\frac{r}{L}\right)^{\zeta_n}, \tag{4}$$

where  $u' \equiv \overline{u^2}^{1/2}$  and  $\zeta_n$  departs from  $n/3$  except when  $n = 3$ , e.g., [1,43–45]. However, as pointed out above, the studies in the last 25 years or so, e.g., [2,3,18–32], indicate that the FRN effect on  $\overline{(\delta u)^n}$  seriously calls into question the validity of the published estimates of  $\zeta_n$ . The first objective of this paper is to review recent advances in understanding the FRN effect on  $\overline{(\delta u)^n}$ . These advances have been underpinned by the use of the transport equations for  $(\delta u)^2$  and  $(\delta u)^3$ .

As described by Antonia et al. [46] and Tang et al. [32] in the context of the transport equation for  $(\delta u)^2$  (or scale-by-scale energy budget), the scaling based on  $(u_K, \eta)$  is effective when the effect of the large-scale term is neglected. This was first pointed out by Batchelor [9]. Also, the transport equation for  $(\delta u)^2$ , when the viscous term is neglected and the large-scale term retained, satisfies similarity when the scaling based on  $(u', L)$  applies. This dual scaling is expected to apply, albeit in an approximate fashion, at finite values of  $Re_\lambda$ . As  $Re_\lambda$  continues to increase, there should be a region of overlap between the two different normalizations. When  $Re_\lambda \rightarrow \infty$ , the IR should be established rigorously, and the two sets of scales should become interchangeable in this range. Tennekes and Lumley [47] and Gamard and George [48] examined the dual scaling in the context of the energy spectrum in a shear flow and grid turbulence, respectively. Their results indicate that IR is likely to emerge at a very large  $Re_\lambda$ . Tang et al. [32] further examined the dual scaling of  $\overline{(\delta u)^n}$  in the context of both the transport equation for  $(\delta u)^2$  and experimental grid turbulence data over a significant range of  $Re_\lambda$ . They show that dual scaling leads to a power-law relation  $\overline{(\delta u)^n} \sim r^{n/3}$  when the inertial range is rigorously established. The latter is likely to occur only when  $Re_\lambda \rightarrow \infty$ . Therefore, the second objective of the present paper is to review the constraints imposed by the dual-scaling approach on the behaviour of  $\overline{(\delta u)^n}$  and energy spectra as  $Re_\lambda \rightarrow \infty$ . It is worth mentioning that Antonia et al. [49], Tang et al. [50] reviewed the FRN effect on small-scale statistics in the dissipative and scaling ranges; the scaling range comprises a range of scales that becomes identifiable with the IR when  $Re_\lambda \rightarrow \infty$ . Research related to the FRN effect, including that by Qian [2,3,18,51], was reviewed in McComb’s [8] monograph, which deals exclusively with HIT. Shi [52] reviewed Qian’s various contributions to small-scale turbulence, including the FRN effect.

**2. Small-Scale FRN Effects**

The FRN effect on  $\overline{(\delta u)^3}$  and  $\overline{(\delta u)^4}$  can be quantified via the following equations of grid turbulence [53]:

$$-\overline{(\delta u^*)^3} = \frac{4}{5}r^* - 6f' - \frac{2}{r^{*4}} \frac{\sqrt{15}}{Re_\lambda} (\Gamma_1 + \frac{1}{2}\Gamma_2), \tag{5}$$

and

$$\overline{(\delta u^*)^4} = 6\Gamma_3 - \Gamma_4 + 2\Gamma_5 + 2\Gamma_6 + \left\{ \frac{1}{3} \frac{\sqrt{15}}{Re_\lambda} (3\Gamma_7 + \Gamma_8) \right\}, \tag{6}$$

where  $\Gamma_1, \Gamma_2, \Gamma_3, \Gamma_4, \Gamma_5, \Gamma_6, \Gamma_7$ , and  $\Gamma_8$  are given by

$$\Gamma_1 = \int_0^{r^*} s^{*4} f(s^*) ds^*, \Gamma_2 = \int_0^{r^*} s^{*5} f'(s^*) ds^* \tag{7}$$

$$\Gamma_3 = \frac{1}{r^{*2}} \int_0^{r^*} s^* E_{uv} f^2 ds^*, \Gamma_4 = \frac{1}{r^{*2}} \int_0^{r^*} s^{*2} T_{111} ds^*. \tag{8}$$

$$\Gamma_5 = \frac{1}{r^{*2}} \int_0^{r^*} s^{*2} E_{111} ds^*, \Gamma_6 = \frac{1}{r^{*2}} \int_0^{r^*} \left( -4 + 4s^* \frac{\partial}{\partial s^*} + s^{*2} \frac{\partial^2}{\partial s^{*2}} \right) S f^{3/2} ds^* \tag{9}$$

$$\Gamma_7 = \frac{1}{r^{*2}} \int_0^{r^*} s^{*2} S f^{3/2} ds^*, \Gamma_8 = \frac{1}{r^{*2}} \int_0^{r^*} s^{*3} \frac{\partial(S f^{3/2})}{\partial s^*} ds^*. \tag{10}$$

In (7)–(10),  $S = \overline{(\delta u)^3} / \overline{(\delta u)^2}^{3/2}$ ;  $E_{uv} = \overline{(\delta u)^2} \overline{(\delta v)^2} / \overline{(\delta u)^2}^2$ ;  $T_{111} = 3 \overline{(\delta u^*)^2} \overline{(\delta \delta p^* / \partial X^*)}$ ;  $E_{111} = 6 \overline{(\delta u^*)} [(\partial u^* / \partial x^*)^2 + 2(\partial u^* / \partial y^*)^2]$ ;  $f = \overline{(\delta u^*)^2}$ ; and the asterisk denotes normalization by the Kolmogorov scales. In deriving (5) and (6), complete similarity was assumed (for convenience) so that similarity applies at all scales of motion, i.e., the exponent  $m$  in  $\overline{u^2} \sim x^m$  must be  $-1$ . In this case,  $Re_\lambda$  must remain constant during the decay, e.g., [25,54–56]. Consequently, and provided  $Re_\lambda$  is sufficiently large, the scaling based on  $(u', L)$  is equivalent to a scaling based on  $(u', \lambda)$  or  $(u_K, \eta)$ , thus justifying the normalization for (5) and (6).

Taking  $r \rightarrow 0$ , the relations that quantified the FRN effect on the skewness and flatness factors of  $\partial u / \partial x$  can be obtained for decaying HIT [53,57,58]. Similar relations for the skewness of  $\partial u / \partial x$  have been obtained in other flows, i.e., along the axis in the far-field of a round jet, the centerline of a fully developed channel flow, the axis in the far-wake of a circular cylinder and forced HIT, e.g., [57].  $Re_\lambda \gtrsim 300$  is sufficient for the skewness of  $\partial u / \partial x$  to reach a constant for the flows mentioned above (see for example Figure 2 of Antonia et al. [49]). The magnitude of the flatness of  $\partial u / \partial x$  increases with  $Re_\lambda$  in grid turbulence and approaches a constant whose magnitude is in approximate agreement with that along the axis in the far-field of the plane and round jets when  $Re_\lambda \gtrsim 600$  [58]. The last term on the right side of (5) is the large-scale term, which involves a cumulative effect (i.e., integration) over all scales ranging from 0 up to  $r$  and leads to the deviation from the four-fifths law at FRN. Similarly, (6) highlights the effect of the large-scale motions, represented by the last term on the right side. Increasing the Reynolds number would help to reduce this effect, as demonstrated by Antonia and Burattini [23], Antonia et al. [30] who showed that  $\overline{(\delta u)^3}$  approaches  $\frac{4}{5} \bar{\epsilon} r$  with increasing  $Re_\lambda$  in homogeneous isotropic turbulence.

Figure 1 shows the variation in the last term on the right side of Equations (5) and (6), divided by  $r^*$  and  $r^{*4/3}$ , respectively. Strictly, the effect of the large scales should be zero before testing K41 and K62. We can observe from this figure that these terms decrease slowly with increasing  $Re_\lambda$ , highlighting the lingering effect of the large-scale motion responsible for the lack of a power-law behaviour for  $\overline{(\delta u)^3}$  and  $\overline{(\delta u)^4}$ . In particular, values of  $Re_\lambda$  between  $10^4$  and  $10^5$  are required before the effect of the large scales (or, equivalently, the FRN effect) disappears. This constraint is entirely consistent with the findings of Tang et al. [32] that dual scaling applies to  $\overline{(\delta u)^n}$  ( $n = 2, 3, 4, 6$ ) and that an overlap range begins to emerge when  $Re_\lambda > 10^4$ ; this will be discussed in the next section.

As discussed above, only when the effect of the large scales becomes negligible over a sufficiently large range of  $r$ , which requires  $Re_\lambda \rightarrow \infty$ , can the 4/5 law (or Equation (2)) be observed convincingly. We recall that Sagaut and Cambon [25] summarized the predictions of Qian [3], Lindborg [19], Moisy et al. [20], Lundgren [21,22] for  $\overline{(\delta u)^3}$  (see their Tables 4.4 and 4.5 where a few empirical models that account for the Reynolds dependency of  $-\overline{(\delta u)^3} / \bar{\epsilon} r$  and the maximum of  $-\overline{(\delta u)^3}$  are displayed). These models, together with the Eddy-Damped Quasi-Normal Markovian (EDQNM) result, the prediction of Antonia and Burattini [23], and experimental and numerical data, are shown in their Figure 4.6. This latter figure was discussed by Meldi et al. [31]. In particular, results based on the EDQNM model of Bos and Bertoglio [59] were presented for both free decaying and forced HIT. These are shown in Figure 2. For the reasons discussed in Meldi et al. [31], we have

not included the grid turbulence data of Comte-Bellot and Corrsin [60] and the EDQNM results of Briard et al. [61] (as reported in Sagaut and Cambon [25]). There is almost perfect agreement between the prediction based on the scale-by-scale budget [23] and the EDQNM [31] in decaying HIT. This is rather impressive in view of the different approaches adopted by Antonia and Burattini [23] and Meldi et al. [31]. Antonia and Burattini [23] used Equation (5) with an empirical model for  $f$  (see their Equation (2.8) , which contains a typo: the power-law exponent  $2c - 2$  in  $(1 + \beta r^*)$ , viz.  $(1 + \beta r^*)^{2c-2}$ , was left out) and a power law for  $\overline{u^2}$ , viz.  $\overline{u^2} \sim x^m$  with  $m = -1.25$ . For Meldi et al. [31], Lin’s transport equation for  $E(\kappa)$  is solved, the initial spectrum having a slope ( $\kappa \rightarrow 0$ ) of 2 (i.e.,  $\sigma = 2$ , which is generally associated with Saffman turbulence [62]), which corresponds to  $m = -1.20$  (note that  $m = -2(\sigma + 1)/(\sigma + 3)$ ). One expects that the green curve in Figure 2 will depend on the choice of  $\sigma$ , at least at small to moderate  $Re_\lambda$ . Similarly, for experimental data, the black curve will depend on the choice of initial conditions; this is confirmed by the trend of the Mydlarski and Warhaft [33] data in Figure 2. As pointed out by Sagaut and Cambon [25], “ $Re_\lambda \geq 50,000$  is required to recover the 4/5 value in freely decaying turbulence, while  $Re_\lambda \geq 5000$  is enough in forced turbulence” (see Figure 2). These results reinforce Antonia and Burattini’s [23] finding that, for decaying HIT,  $Re_\lambda$  should probably exceed  $10^6$  before the IR for  $(\delta u)^3$  is established unequivocally, Qian’s [2] prediction that  $Re_\lambda$  should be higher than  $10^4$  in order to have an IR wider than one decade for  $(\delta u)^3$ , and the predictions of Antonia et al. [30] and Tang et al. [32] that the values of  $Re_\lambda$  between  $10^4$  and  $10^5$  are required before one can claim an IR for  $(\delta u)^n$  ( $n = 2, 3, 4, 6$ ) of modest extent. Evidently, the values of  $Re_\lambda$  for the establishment of an IR suggested by the above authors are currently beyond the reach of the experiments and direct numerical simulations. Although there is no doubt that, for forced turbulence,  $-(\delta u)^3/\bar{\epsilon}r$  reaches 4/5 at a smaller  $Re_\lambda$  than for decaying turbulence, a clear plateau for  $(\delta u)^2/(\bar{\epsilon}r)^{2/3}$  cannot be observed. In particular, the distribution for this quantity exhibits a relatively sharp rise towards the upper end of the scaling range when forcing is applied. This clearly affects the slope  $d \log((\delta u)^2)/d \log r$ , as can be seen in Figure 9 of Meldi et al. [31] where the largest  $Re_\lambda$  is  $10^6$ . Mainly, on the basis of this result, Meldi et al. [31] inferred that conclusions drawn from forced turbulence studies do not necessarily apply to decaying turbulence and vice versa.

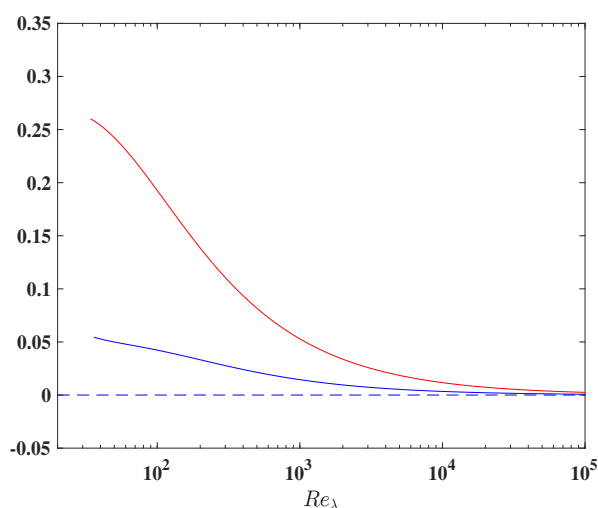


**Figure 1.**  $Re_\lambda$  variation in the last term on the right side of Equation (5) (red curve) and the last term on the right side of (6) (blue curve), divided by  $r/\eta$  and  $(r/\eta)^{4/3}$ , respectively, at  $r = \lambda$  in grid turbulence. The red curve has already been reported in Tang et al. [29] (see their Figure 7). This figure is reproduced from Figure 5 of Djenidi et al. [53] with permission.

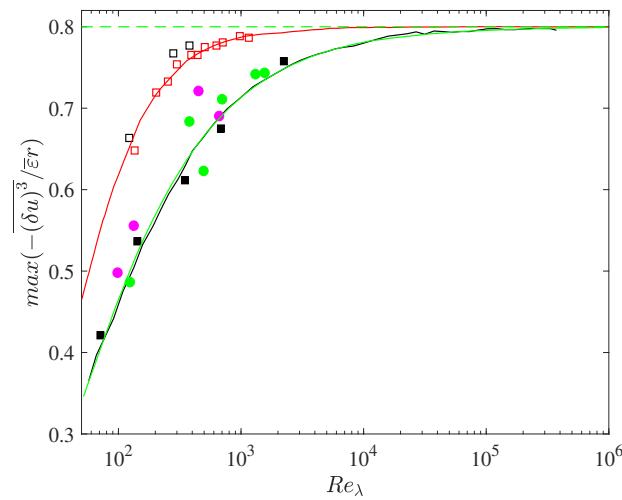


**Figure 2.** Maximum values of  $-\overline{(\delta u)^3}/\bar{\epsilon}r$  in decaying (solid symbols) and forced (open symbols) HIT. ( $\square$ ), Moisy et al. [20]; ( $\square$ ) [63]; ( $\blacksquare$ ) Gagne et al. [64]; ( $\bullet$ ), Mydlarski and Warhaft [33]; ( $\bullet$ ), estimated from Figure 12 of Tang et al. [32], which was originally measured by Bodenschatz et al. [36]. The black curve was calculated from the scale-by-scale budget [23]. The red and green curves correspond to the EDQNM results of Meldi et al. [31].

### 3. Dual Scaling and Its Constraints

It is now well established that the requirements for complete similarity or complete self-preservation of decaying HIT via the KH equation or the Lin equation are quite stringent, e.g., [25,56,65,66]. The only way to achieve complete self-preservation, i.e., self-preservation at all scales, is for  $Re_\lambda$  to remain constant during the decay and for the slope  $\sigma$  of the spectrum in the infrared range of the spectrum, i.e.,  $E(\kappa \rightarrow 0) \sim \kappa^\sigma$  (the prefactor does not depend on time  $t$ ), to be equal to 1. The corresponding requirement in physical space is that, e.g., [67]  $f(r \rightarrow \infty) \sim r^{-2}$  ( $f$  is the two-point velocity correlation; the prefactor does not depend on  $t$ ). It follows that the invariant is  $\overline{u^2}\lambda^2$ , which simply reflects the requirement that  $Re_\lambda$  must remain constant during the decay. Using EDQNM closure, Meldi and Sagaut [56] provided excellent support for the “−1” rate of decay (i.e.,  $\overline{u^2} \sim t^{-1}$ ) when  $\sigma = 1$  and  $Re_\lambda$  is constant (starting from the initial time), regardless of the initial value of  $Re_\lambda$ , i.e., independently of whether the decay is in its initial period or its final period.

Since the above requirements are not physically realizable, a more reasonable approach is to consider incomplete or partial self-preservation. This leads almost naturally to considering a dual-scaling approach, which is physically realizable, where self-preservation is now satisfied at either small  $\kappa$  or large  $\kappa$  for the Lin equation or small  $r$  or large  $r$  for the KH equation. We discuss this in (Section 3.1) in the context of the Lin equation and in (Section 3.2) in the context of the scale-by-scale energy budget, which corresponds to the KH equation.

#### 3.1. Dual Scaling of the Energy Spectrum

Tennekes and Lumley [47] first examined a dual scaling of the energy spectrum  $E(\kappa)$ , i.e., a scaling based on the Kolmogorov scales ( $u_\kappa, \eta$ ) and another based on ( $u', L$ ) representative of the large-scale motion in a shear flow. The starting point is the recognition that the small and large wavenumber portions of  $E(\kappa)$ , the 3D energy spectrum, scale differently. The high wavenumber end of the spectrum should scale on Kolmogorov scales, viz.

$$\frac{E(\kappa)}{\nu^{5/4}\bar{\epsilon}^{1/4}} = \frac{E(\kappa)}{u_\kappa^2\eta} = f(\kappa\eta). \tag{11}$$

For small wavenumbers, the principal parameters are the mean strain rate  $S$ , assumed to be  $u'/L$ , and the rate, assumed to be  $\bar{\epsilon}$  ( $\equiv u'^3/L$ ), at which energy is transferred from large to small scales, i.e.,  $E(\kappa)$  is now described by

$$\frac{E(\kappa)}{\bar{\epsilon}^{3/2}S^{-5/2}} = \frac{E(\kappa)}{u'^2L} = F(\kappa L), \tag{12}$$

where  $S = u'/L$ . Equating (11) and (12) leads to a solution

$$E(\kappa) = \alpha \bar{\epsilon}^{2/3} \kappa^{-5/3}, \tag{13}$$

where  $\alpha$  is the Kolmogorov (Obukhov) constant. Tennekes and Lumley [47] use  $\kappa L = 367$  and  $\kappa\eta \approx 0.05$  to delineate the boundaries of the inertial range. Their Figure 8.6 is replotted in Figure 3 where we have used  $Re_\lambda$  ( $\equiv 15^{1/2}R_L^{1/2}$ ) instead of  $R_L$ , mainly because, from an experimental perspective,  $\lambda$  can be determined more accurately than  $L$ . The intersection of the two lines is at  $Re_\lambda = 1425$ .  $Re_\lambda$  would need to be at least one order of magnitude larger than this value before one could claim to have an inertial range of significant extent. We realise there is unavoidable arbitrariness in constructing Figure 3. Nonetheless, the delineated region is not implausible and, as concluded by Tennekes and Lumley [47], highlights the difficulty in encountering an inertial range in laboratory flows. Gamard and George [48] used this dual-scaling approach to describe how the longitudinal velocity spectrum, as measured by Mydlarski and Warhaft [33] in grid turbulence, evolves with  $Re_\lambda$  in the overlap region. They observe that the scaling based on  $(u_\kappa, \eta)$  extends to increasingly smaller values of  $\kappa_1\eta$ . In contrast, the scaling based on  $(u', L)$  extends to increasingly more significant values of  $\kappa_1L$  as  $Re_\lambda$  increases (see, for example, Figure 3 of Gamard and George [48]). Such a feature can also be observed in Figure 4, which shows distributions of the one-dimensional energy spectra, normalized by  $(u', L)$  and  $(u_\kappa, \eta)$ , in grid turbulence at  $Re_\lambda = 110\text{--}1450$ . Here, the maximum  $Re_\lambda$  is much larger than that of Gamard and George [48] where the maximum  $Re_\lambda$  is 470. More importantly, both scalings should eventually overlap in the inertial range over which Equation (13) is valid as  $Re_\lambda$  continues to increase. This can be confirmed by Figure 5, which shows the  $(u', L)$  and  $(u_\kappa, \eta)$  normalized energy spectra in decaying isotropic turbulence using the EDQNM model at  $Re_\lambda = 10^3, 10^4$ , and  $10^5$ , respectively. In particular, at  $Re_\lambda = 10^4$  and  $10^5$ , the upper value of  $\kappa L$  exceeds  $10^4$ , whilst the lower value of  $\kappa\eta$  lies below  $10^{-4}$ . Taking  $Re_\lambda = 5 \times 10^4$  and using the isotropic relation  $\frac{L}{\eta} = C_\epsilon \frac{Re_\lambda^{3/2}}{15^{3/4}}$  with  $C_\epsilon = 0.8$  [32], we can estimate that the overlap region is given by  $10^{-4} \lesssim \kappa\eta \lesssim 8.5 \times 10^{-3}$ . Evidently, a distinct “ $(\kappa^{-5/3})$ ” range of overlap, smaller than two decades, between the  $(u', L)$  and  $(u_\kappa, \eta)$  scalings can be observed at  $Re_\lambda = 10^4$  and  $10^5$ . A similar behaviour can be observed in Figure 3 at a comparable  $Re_\lambda$ . The overlap region in Figure 5 is unlikely to depend on the choice of the spectrum slope parameter  $\sigma$  ( $E(\kappa \rightarrow 0) \sim \kappa^\sigma$ ), at least for  $\sigma = 1$  to 4; the choice of  $\sigma$  only affects the distributions in the range  $0 \lesssim \kappa L \lesssim 1$ . Note that  $\sigma = 2$  corresponds to what is described as Saffman turbulence [62], whilst  $\sigma = 4$ , which is based on the Loitsiansky invariant [68], is generally referred to as Batchelor turbulence (see Batchelor [55]). Gamard and George [48] used this dual-scaling approach to describe how the longitudinal velocity spectrum, as measured by Mydlarski and Warhaft [33] in grid turbulence, evolves with  $Re_\lambda$  in the overlap region. In the scale range of Gamard and George [48] at finite Reynolds numbers, the spectrum was assumed to vary, albeit approximately, as  $\alpha \kappa_1^{-5/3+\beta}$ , where  $\alpha$  and  $\beta$  depend on  $Re_\lambda$ . In the limit  $Re_\lambda \rightarrow \infty$ ,  $\beta \rightarrow 0$  and  $\alpha \rightarrow \text{constant}$ , and thus (13) is established. Figure 6 shows the dependence of the difference  $(5/3 - \beta)$  on  $Re_\lambda$  in grid turbulence. The “ $-5/3$ ” power-law scaling is approached slowly as  $Re_\lambda$  increases. This is further confirmed by the local slope  $(LS_E = d \log(E(\kappa))/d \log \kappa)$  in decaying isotropic turbulence using the EDQNM model at  $Re_\lambda = 204, 471, 1131, 10^4, 10^5$ , and  $10^6$ , respectively (Figure 7a).

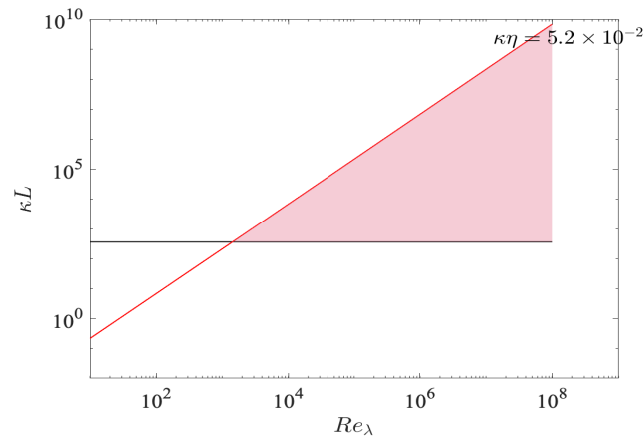


**Figure 3.** The emergence of an inertial subrange (red region) in the context of the energy spectrum with increasing  $Re_\lambda$ . The two lines correspond to  $\kappa L = 367$  and  $\kappa\eta = 0.052$ , respectively. This figure is similar to Figure 8.6 of Tennekes and Lumley [47] except we have used  $Re_\lambda$  instead of  $R_L$ .

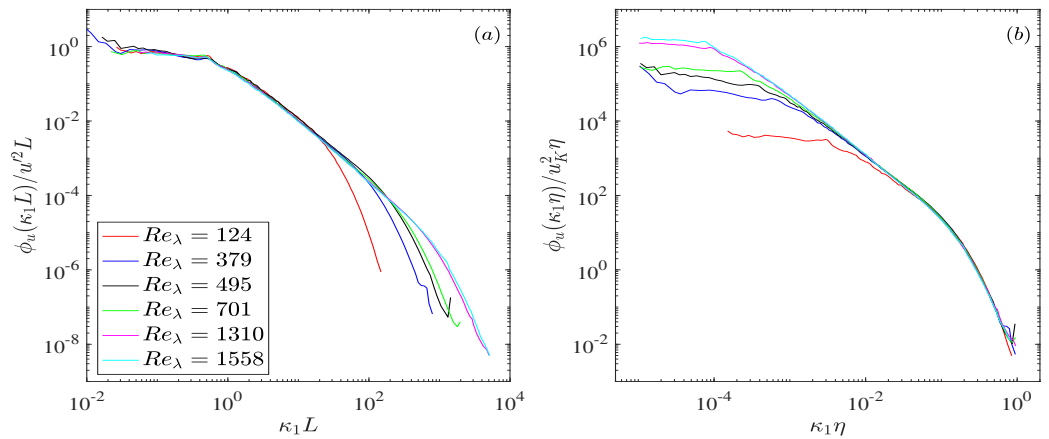


**Figure 4.** (a) Distributions of one-dimensional energy spectra  $\phi_u(\kappa_1)$ , normalized by  $(u', L)$ , in grid turbulence at  $Re_\lambda = 110$ – $1450$ ; they are plotted using the data in Figure 1a of Tang et al. [32], originally measured by Bodenschatz et al. [36]. (b) Corresponding distributions normalized by  $(u_K, \eta)$ .

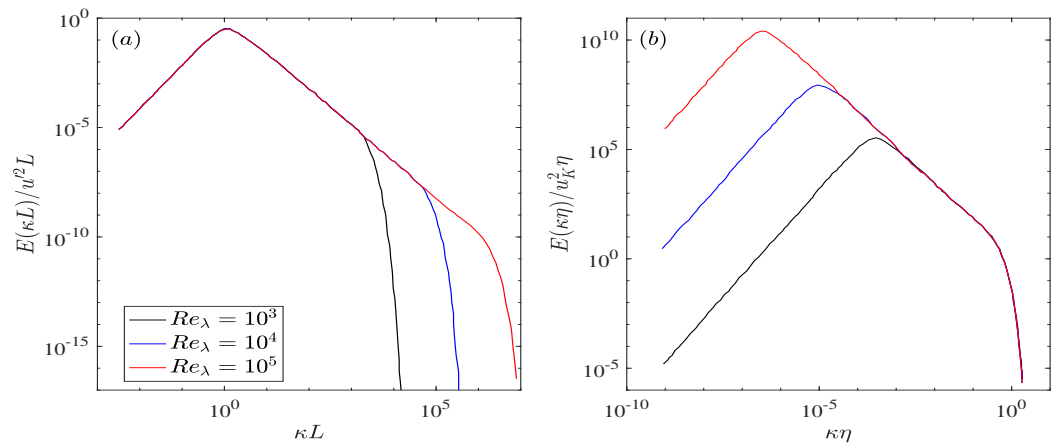


**Figure 5.** (a) Distributions of three-dimensional energy spectra  $E(\kappa)$ , normalized by  $(u', L)$ , in decaying isotropic turbulence using the EDQNM model at  $Re_\lambda = 10^3, 10^4$ , and  $10^5$ , respectively. (b) Corresponding distributions normalized by  $(u_K, \eta)$ . They are plotted using the data in Figures 5a,g of Meldi and Sagaut [56]. The curves correspond to  $\sigma = 2$ .

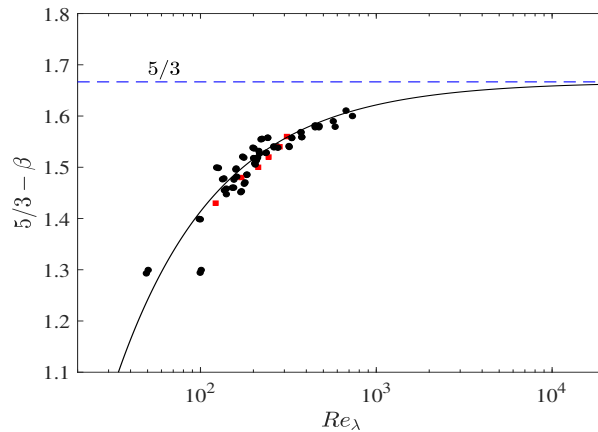


**Figure 6.**  $5/3 - \beta$  ( $\phi_u(\kappa_1) \sim \kappa_1^{-(5/3-\beta)}$ ) in grid turbulence (■ [33]; ● [34]). Dashed horizontal line:  $5/3$ . Black empirical curve,  $5/3 - 8Re_\lambda^{-3/4}$  [34].

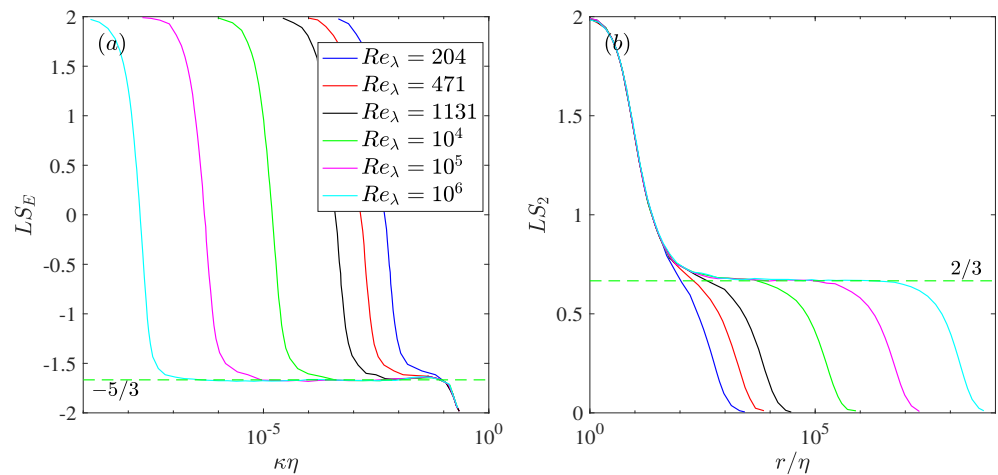


**Figure 7.** (a) Local slope ( $LS_E = d \log(E(\kappa))/d \log \kappa$ ) in decaying isotropic turbulence using the EDQNM model at  $Re_\lambda = 204, 471, 1131, 10^4, 10^5,$  and  $10^6,$  respectively. Dashed horizontal line:  $-5/3$ . (b) Local slope ( $LS_2 = d \log(\overline{(\delta u)^2})/d \log r$ ) corresponding to (a). Dashed horizontal line:  $2/3$ . They are plotted using the data in Figures 2 and 9a of Meldi et al. [31].

### 3.2. Dual Scaling of the Scale-by-Scale Energy Budget

The transport equation for  $\overline{(\delta u)^2}$  is given by

$$\frac{4}{5} \overline{\epsilon} r = -\overline{(\delta u)^3} + 6\nu \frac{\partial}{\partial r} \overline{(\delta u)^2} - \frac{3}{r^4} \int_0^r s^4 \left[ U \frac{\partial \overline{(\delta u)^2}}{\partial x} \right] ds, \tag{14}$$

where  $U$  is the mean (constant) velocity in the  $x$  direction and the last term reflects the contribution from the large scales to the transport of  $\overline{(\delta u)^2}$  in homogeneous and isotropic turbulence, e.g., [5,69]. Normalizing Equation (14) by Kolmogorov scales and assuming  $\overline{u^2} \sim x^m$  with  $m = -1$  lead to Equation (5).

Tang et al. [32], Antonia et al. [46] examined the conditions for which Kolmogorov scaling ( $u_K, \eta$ ) satisfies the similarity of Equation (14). Briefly, when the effect of the large-scale term (the last term in Equation (14)) is neglected, Equation (14) can be rewritten as

$$\frac{4}{5} \frac{r}{l_0} = \frac{6\nu u_0^2}{\overline{\epsilon} l_0^2} f' - \frac{u_0^3}{\overline{\epsilon} l_0} g\left(\frac{r}{l_0}\right), \tag{15}$$

when the  $(u_K = u_0, \eta = l_0)$  scaling applies (here, the prime signifies a derivative with respect to  $r/l_0$ ), so that  $\bar{\epsilon}l_0/u_0^3$  and  $\bar{\epsilon}l_0^2/\nu u_0^2$  (or  $\bar{\epsilon}l_0/u_0^3, u_0l_0/\nu$ ) are constants. Clearly,  $(u_K, \eta)$  is a possible solution since

$$\frac{\bar{\epsilon}\eta}{u_K^3} = 1 \quad \text{and} \quad \frac{u_K\eta}{\nu} = 1. \tag{16}$$

Tang et al. [32] also examined the conditions for which the scaling based on  $(u', L)$  satisfies the similarity of Equation (14). When the large-scale term (the last term in Equation (14)) is retained and the viscous term is neglected, Equation (14) can be rewritten as

$$\frac{4}{5} \frac{r}{l_0} = -\frac{u_0^3}{\bar{\epsilon}l_0} g\left(\frac{r}{l_0}\right) + \frac{3}{(r/l_0)^4} \left( \int_0^{r/l_0} \left(\frac{s}{l_0}\right)^4 f\left(\frac{r}{l_0}\right) \frac{ds}{l_0} \right) \left[ \frac{U}{\bar{\epsilon}} \frac{\partial u_0^2}{\partial x} - \frac{Uu_0^2}{\bar{\epsilon}} \left(\frac{r}{l_0}\right)^2 \frac{f'}{l_0} \frac{dl_0}{dx} \right]. \tag{17}$$

The first term within square brackets is constant since  $\bar{\epsilon} = -\frac{3}{2}U \frac{\partial u_0^2}{\partial x}$  is the turbulent energy budget (when  $u_0 \equiv u'$ ). The coefficient of the second term, i.e.,  $\frac{Uu_0^2}{\bar{\epsilon}} \frac{dl_0}{dx}$ , is also constant with the  $(u', L)$  scaling since the normalized dissipation rate  $\bar{\epsilon}L/u'^3$  is constant and  $\frac{1}{u'} \frac{dL}{dx}$  is also constant as both  $u'$  and  $dL/dx$  vary as  $x^{m/2}$  when the energy decays according to a power law, viz.  $\bar{u}^2 \sim x^m$  and  $\bar{\epsilon} \sim x^{m-1}$ . It is worth mentioning that the  $(u', L)$  scaling may depend on the flow types since  $\bar{\epsilon}L/u'^3$  differs from flow to flow (see for example Figure 2 of [32]). Even in a given flow such as grid turbulence, the  $(u', L)$  scaling may also depend on the initial conditions.

The above considerations indicate that similarity based on  $(u_K, \eta)$  can satisfy (15) when  $r$  is sufficiently small. This is supported by the grid turbulence data in Figure 8a over a significant range of  $Re_\lambda$ . Equally, (17) admits a similarity solution based on  $(u', L)$  when  $r$  is sufficiently large, which is supported by the grid turbulence data in Figure 8b. Since both scalings must eventually overlap as  $Re_\lambda \rightarrow \infty$ , the overlap region should include the inertial range. Regardless of the scaling used, this overlap region should satisfy similarity and hence be independent of  $Re_\lambda$ , which leads to a '2/3' power-law scaling for  $(\delta u)^2$  [32]. This result was also derived by Lundgren [21] from the Karman–Howarth equation using matched asymptotic expansions when  $Re_\lambda \rightarrow \infty$ . A similar result was derived earlier by Gamard and George [48] in the context of the  $u$  spectrum; the approach adopted in this paper is consistent with the asymptotic invariance principle and the methodology of near-asymptotics, introduced by George [70,71]. We recall that Ni and Xia [27] examined the prefactors of  $(\delta u)^2$  ( $A_2$ ) and the one-dimensional energy spectrum ( $\alpha$ ) in the scaling range for various flows, e.g., in the central region of a cylindrical Rayleigh–Benard turbulent convection cell, an axisymmetric jet, a turbulent boundary layer and a stationary forced periodic box turbulence over a large range of  $Re_\lambda$  ( $=55\sim 1450$ ). They found that all prefactors of  $(\delta u)^2$  and spectra in these flows depend on  $Re_\lambda$  and the type of flow. In particular, they found that  $\alpha/A_2 - 0.25 = 1.95Re_\lambda^{-0.68}$  and the widely used relation  $A_2 = 4.02\alpha$  holds only when  $Re_\lambda \gtrsim 10^5$ . These results are consistent with the dual-scaling approach outlined in this paper. It is worth mentioning that the IR in real space should be much shorter than that in wavenumber space [27]. This can also be inferred from the local slopes for  $E(\kappa)$  (Figure 7a) and for  $(\delta u)^2$  (Figure 7b) in decaying isotropic turbulence using the EDQNM model at  $Re_\lambda = 204, 471, 1131, 10^4, 10^5$ , and  $10^6$ , respectively. In a recent paper, Kuchler et al. [40] examined the behaviour of  $(\delta u)^2$  and  $(\delta u)^3$  in grid turbulence at very large  $Re_\lambda$  ( $=2680\sim 5779$ ). One important conclusion is that they do not observe power laws for  $(\delta u)^2$ , even at  $Re_\lambda = 5779$ . Actually, their  $-(\delta u)^3/(\bar{\epsilon}r)$  distributions also do not show a plateau (see their figure 1) at the same  $Re_\lambda$ . Such a behaviour is fully consistent with the above observations in the context of Figures 2 and 7b that much larger values of  $Re_\lambda$ , beyond the

reach of the present experiments, are required to establish the power laws for  $\overline{(\delta u)^2}$  and  $\overline{(\delta u)^3}$  in freely decaying turbulence.

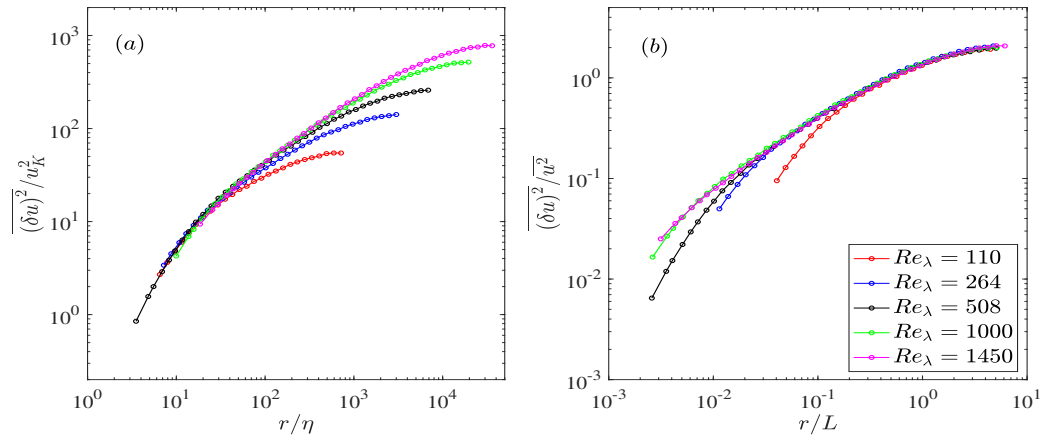


**Figure 8.** (a) Distributions of  $\overline{(\delta u)^2}$ , normalized by  $(u_K, \eta)$  in grid turbulence. (b) Corresponding distributions normalized by  $(u', L)$ . This figure is reproduced from Figure 6 of Tang et al. [32] with permission; the data are originally measured by Kaminsky et al. [39].

We stress that the above dual-scaling approach can be extended to higher orders, which leads to a power-law relation  $\overline{(\delta u)^n} \sim r^{n/3}$  when  $Re_\lambda \rightarrow \infty$  [32]. In particular, Tang et al. [32] compared an empirical model for  $\overline{(\delta u)^n}$  ( $n = 2, 3, 4, 6$ ), i.e.,

$$\frac{\overline{(\delta u)^n}}{u_K^n} = \frac{1}{15^{n/2}} F_n \frac{\left(\frac{r}{\eta}\right)^n (1 + D_n \left(\frac{r}{L}\right))^{2C_n - n}}{\left(1 + B_n \left(\frac{r}{\eta}\right)^2\right)^{C_n}}, \tag{18}$$

where  $B_n, C_n, D_n$ , and  $F_n$  are constants (they are given in Tables 2 and 3 of Tang et al. [32] except for  $C_n (= n/3)$ , which is justified in Tang et al. [32]) with grid turbulence data over a significant range of  $Re_\lambda$ . The model, which is consistent with  $\overline{(\delta u)^n} \sim r^{n/3}$  as  $Re_\lambda \rightarrow \infty$ , is in reasonable accord with the data for values of  $Re_\lambda$  up to about 1500, thus allowing extrapolation of the model-based results to larger values of  $Re_\lambda$ . As an example, we show in Figure 9a the distributions of  $\overline{(\delta u)^4} / (\bar{\epsilon}r)^{4/3}$  based on an empirical model for  $\overline{(\delta u)^4}$  at  $Re_\lambda = 110, 264, 508, 1000, 1450, 10^4$ , and  $10^5$ , respectively. Also shown are the corresponding grid turbulence data, measured by Kaminsky et al. [39]. Figure 9b shows the corresponding local slope  $LS_4 (= d \log(\overline{(\delta u)^4}) / d \log r)$ . There is strictly no power-law range for the experimental data of  $\overline{(\delta u)^4}$ , even at  $Re_\lambda \sim 1500$ . It is evident that the local slope  $LS_4$  continues to evolve with  $Re_\lambda$  (Figure 9b) and begins to exhibit a small plateau only when  $Re_\lambda$  exceeds  $10^4$ . An important inference from this trend is that the grid turbulence data are consistent with (3).

Using the Hölder inequality, Djenidi et al. [72] derived a constraint for  $\overline{(\delta u)^n}$ , i.e.,

$$(p_3 - p_1)\zeta_{2p_2} = (p_3 - p_2)\zeta_{2p_1} = (p_2 - p_1)\zeta_{2p_3}, \tag{19}$$

where  $\overline{(\delta u)^n} \sim r^{\zeta_n}$  and  $p_1 \leq p_2 \leq p_3$  are any three positive numbers. Equation (19) leads to  $\zeta_{2n} = n\zeta_2$  when taking  $p_1 = 0, p_2 = 1$ , and  $p_3 = n$ . This indicates that the power-law exponents of an even order increase linearly with  $n$ . More importantly, using the Cauchy–Schwarz inequality, which is a special case of the Hölder inequality, and the 4/5-law, they further derived  $\zeta_n = n/3$  when  $Re_\lambda \rightarrow \infty$ , i.e., the prediction of K41.

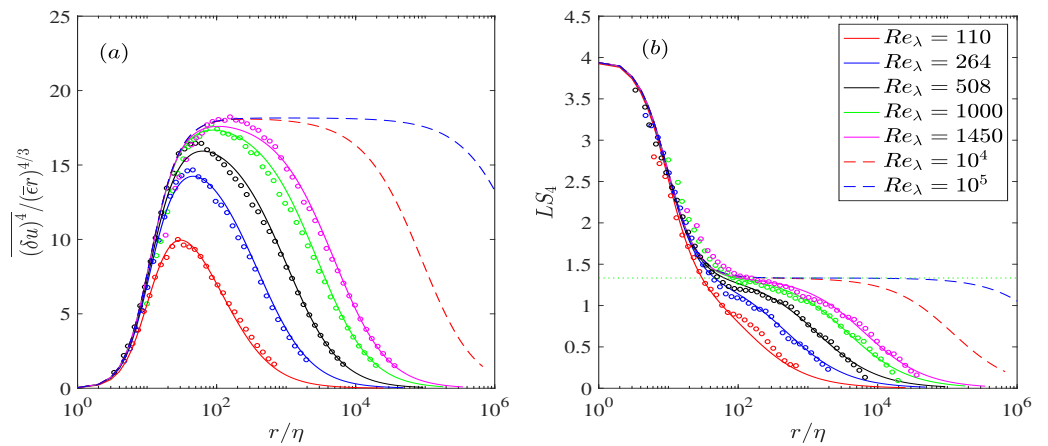


**Figure 9.** (a) Distributions of  $\overline{(\delta u)^4} / (\bar{\epsilon}r)^{4/3}$  based on an empirical model for  $\overline{(\delta u)^4}$  at  $Re_\lambda = 110, 264, 508, 1000, 1450, 10^4,$  and  $10^5$ , respectively [32]. Symbols with the same color are the corresponding grid turbulence data [39]. (b) Local slope ( $LS_4 = d \log(\overline{(\delta u)^4}) / d \log r$ ) corresponding to the distributions in (a). Dashed horizontal line:  $4/3$ . This figure is reproduced from Figure 13 of Tang et al. [32] with permission.

It is worth mentioning that, based on the assumption of local homogeneity and local isotropy, the pressure structure function can be written solely in terms of the fourth-order velocity structure functions [73]

$$D_p(r) = -\frac{1}{3}D_{1111}(r) + \frac{4}{3}r^2 \int_r^\infty y^{-3} [D_{1111}(y) + D_{\chi\chi\chi\chi}(y) - 6D_{11\gamma\gamma}(y)] dy + \frac{4}{3} \int_0^r y^{-1} [D_{\chi\chi\chi\chi}(y) - 3D_{11\gamma\gamma}(y)] dy, \tag{20}$$

where  $D_p(r)$  is the pressure structure function,  $D_{1111}(r) = \overline{(\delta u)^4}$ , and  $\chi$  and  $\gamma$  stand for 2 or 3. Since dual scaling applies to the fourth-order velocity structure functions [32], one would expect, based on Equation (20), that dual scaling will also apply to  $D_p(r)$  and, concomitantly, the pressure spectrum  $E_p(\kappa)$ . This would lead to  $D_p(r) \sim r^{4/3}$  and  $E_p(\kappa) \sim \kappa^{-7/3}$  in the overlap region when  $Re_\lambda \rightarrow \infty$ . Indeed, the EDQNM results of Meldi and Sagaut [74] in decaying HIT confirmed that there are about three decades of IR in the pressure spectrum with a K41  $-7/3$  [75] scaling at  $Re_\lambda = 10^6$  (see their Figure 2).

#### 4. Dual Scaling for Higher-Order Even Moments of $\delta u$

A final comment is devoted to the scaling of higher-order, even longitudinal structure functions  $\overline{(\delta u)^n}$ , for  $n = 4, 6, 8, \dots$ , in the context of the dual scaling approach. Transport equations of these higher-order structure functions were developed by Peters et al. [76] and showed that dissipative effects are reflected in complex terms, involving correlations between the energy dissipation rate and lower-order moments of velocity increments. Furthermore, Boschung et al. [77] introduced exact dissipative scales for the even-order longitudinal structure functions. The derivation was based on exact relations between even-order moments of the longitudinal velocity gradient  $\overline{(\partial u / \partial x)^n}$  and  $\overline{\epsilon^{n/2}}$ . Boschung [78] related moments of the dissipation rate to moments of the longitudinal velocity derivatives, which simplifies to some extent the assessment of different terms in the transport equations.

The similarity length scale was shown to be  $\eta_{g,n} = (v^3 / \overline{\epsilon^{n/2}}^{2/n})^{1/4}$ , where the subscripts ‘g’ and ‘n’ stand for ‘generalized’ and ‘n’-th order, respectively. The velocity scale is  $u_{g,n} = (v \overline{\epsilon^{n/2}}^{2/n})^{1/4}$ , i.e., the dissipative scales depend on the moments of  $\overline{\epsilon^{n/2}}$  and not on the mean value of the dissipation rate itself. The derivations are exact for longitudinal even-ordered structure functions under the assumptions of (local) isotropy, (local) homogeneity, and incompressibility. Direct numerical simulations (DNS) for Reynolds numbers

up to  $Re_\lambda = 754$  were used to validate the generalized scalings. The generalized, order-dependent viscous scales  $\eta_{g,n}$  are cut-off length scales that are smaller than  $\eta$  and decrease with increasing order and Reynolds number [77]. Gauding et al. [79] have extended the approach for the scalar field fed by a large-scale mean scalar gradient and revealed that the appropriate similarity scales for the dissipative range are based on the  $n$ -th power of the scalar dissipation rate.

In the following, we show that the dual-scaling approach, combined with the similarity scales  $\eta_{g,n}$  and  $u_{g,n}$  previously defined, are consistent with a scaling for the  $n$ -th-order structure function of the longitudinal velocity component  $(\delta u)^n \sim r^{n/3}$ . In other words, the  $n/3$  scaling, although conditioned by extremely high values of the Reynolds number, is robust with respect to the particular choice of the small-scale similarity scales. Specifically, the dual scaling requires small scales to be universal when appropriately normalized with respect to  $\eta_{g,n}, u_{g,n}$ , whereas for very large scales, the characteristic scale is  $\mathcal{L}$  (to be defined) and  $u'$ , a typical velocity. The final result is

$$\frac{u'^n}{u_{g,n}^n} \sim \left( \frac{\mathcal{L}}{\eta_{g,n}} \right)^{C_n} \tag{21}$$

We now need to ascertain the dependence of  $C_n$  on  $n$ . Specific to higher-order moments, the definition of  $\mathcal{L}$  should comply with the large-scale limit of the transport equation of  $(\delta u)^n$ , which is

$$\frac{u'^{n+1}}{\mathcal{L}} \sim \overline{u'^{n-2}\epsilon}, \tag{22}$$

which is obviously consistent for  $n = 2$  with the definition of  $C_\epsilon$ . Note that there is no reason to use the classical normalized dissipation rate  $C_\epsilon = 1$  in the context of higher-order moments. Indeed,  $\bar{\epsilon}$  is the destruction rate of the kinetic energy (i.e., the second-order moments), whereas we need the destruction rate of the  $n$ -th-order moment, which is  $\overline{u'^{n-2}\epsilon}$  (the transport equation of  $u$  is multiplied by  $u'^{n-1}$  resulting finally in a dissipative term  $\overline{u'^{n-2}\epsilon}$ ). This appears to be a distinct point with respect to other previous approaches. Furthermore, the right-hand side of Equation (22) can be written as

$$\overline{u'^{n-2}\epsilon} \sim \epsilon^{\frac{n-2}{2}+1} \left( \frac{\mathcal{L}}{u'} \right)^{\frac{n-2}{2}} \tag{23}$$

The one-point budget of  $u^n$  scales as

$$\overline{u'^{n-2}\epsilon} \sim \frac{u'^{n+1}}{\mathcal{L}}. \tag{24}$$

Equations (23) and (24) lead to

$$\mathcal{L} \sim \frac{u'^3}{\epsilon^{n/2+2/n}}, \tag{25}$$

which fully complies for  $n = 2$  with the classical  $C_\epsilon$  definition. Injecting (25) into Equation (21) results in  $C_n = n/3$ , which is fully robust with respect to the choice we made for both small and large scales. The basic assumptions made stand in selecting scales that comply with the definition per se of the  $n$ -th-order moment at very small scales (therefore based upon the  $n/2$ -th order of the dissipation), and with the large-scale limits of the transport equation for the  $n$ -th-order structure functions, i.e., the one-point budget of the  $n$ -th-order moment.

### 5. Concluding Remarks

We have reviewed relatively recent work in connection with the effect of  $Re_\lambda$  on a range of scales, which eventually becomes identifiable with the inertial range, when  $Re_\lambda$

reaches very large values. The focus has been mainly on HIT and the various constraints that act on this range of scales.

The main conclusions that can be drawn from this review are as follows:

- (i) K41 and K62 require the effect of the large scales on the small scales to be negligible. Analytical considerations in the context of the transport equations of  $\overline{(\delta u)^2}$  and  $\overline{(\delta u)^3}$  in decaying grid turbulence (Equations (5) and (6) and Figure 1) indicate that values of  $Re_\lambda$  between  $10^4$  and  $10^5$  are required before the effect of the large scales (or equivalently, the FRN effect) disappears. Consequently, Equation (2), i.e., the 4/5 law, will be validated when the large-scale (or non-stationary) term in (5) is no longer important. This is confirmed by the experimental data and EDQNM results in Figure 2.
- (ii) The results, inferred from the dual-scaling approach, based on either the energy spectra or the scale-by-scale energy budget are consistent with those in (i). For the scale-by-scale energy budget in decaying HIT, the  $(u_\kappa, \eta)$  scaling at small scales should be effective since the two dimensionless parameters in Equation (16) are universal (by definition). The  $(u', L)$  scaling should also be tenable for both large scales and scales within the scaling range since both  $\bar{\epsilon}L/u'^3$  and  $\frac{1}{u'} \frac{dL}{dx}$  should approach constant values as  $Re_\lambda$  increases. The dual-scaling approach, which satisfies incomplete similarity of (5), is supported by the experimental data and the EDQNM results (Figures 4 and 5); it is also supported by the  $\overline{(\delta u)^n}$  ( $n = 2, 3, 4, 6$ ) distributions in grid turbulence over a significant range, in the context of laboratory measurements, of  $Re_\lambda$  [32]. When  $Re_\lambda$  is sufficiently large, both scalings should overlap, thus leading to the power-law relations  $\overline{(\delta u)^n} \sim r^{n/3}$  and  $E(\kappa) \sim \kappa^{-5/3}$  in the overlap region over which the inertial range is established. This is consistent with the constraints imposed by the Hölder and Cauchy–Schwarz inequalities [72]. The EDQNM results of Meldi et al. [31] (Figure 7), the empirical fit of Mydlarski and Warhaft [33,34] for the energy spectra (Figure 6), and the extrapolation of Tang et al. [32] for  $\overline{(\delta u)^n}$  ( $n = 2, 3, 4, 6$ ) (Equation (18); see also Figure 9 for  $n = 4$ ) indicate that values of  $Re_\lambda$  between  $10^4$  and  $10^5$  are required before an overlap range begins to emerge. Evidently, the maximum values of  $Re_\lambda$  that are achievable in laboratory experiments and direct numerical simulations are, as yet, insufficient to observe a power-law behavior of significant extent in energy spectra and, more especially,  $\overline{(\delta u)^n}$ . McComb [8] concluded the discussion in chapter 6 of his monograph with “our view is that K41 is basically correct and that, in particular, the work of Gamard and George [48] and of Lundgren [21], when taken together, leave little room for doubt on this matter”. The EDQNM results (Figure 7) at very high  $Re_\lambda$  and those obtained by extrapolation, via Equation (18) to comparably high values  $Re_\lambda$  (Figure 9), reinforce McComb’s conclusion.

It is worth mentioning that there has been strong support for  $(u_\kappa, \eta)$  scaling in the context of the energy spectra in the dissipative range in various flows (see for example Figure 9 of Saddoughi and Veeravalli [80], Figure 6.14 of Pope [81], Figure 3 of Gotoh et al. [63], Figure 5 of Larssen and Devenport [82], Figures 1 and 2 of Antonia et al. [46], and Figure 1a of Tang et al. [83]). However, a departure from this scaling has been noted in stationary forced periodic box turbulence at relatively high  $Re_\lambda$  [84–87], the Kolmogorov-normalized energy spectra increasing systematically (for  $\kappa \gtrsim 0.5$ ) with increasing  $Re_\lambda$ . Concomitantly, although the skewness of  $\partial u/\partial x$  ( $S_{\partial u/\partial x}$ ) in this flow is constant for  $Re_\lambda = 70 \sim 300$ , it starts to increase slowly with  $Re_\lambda$ , when the latter exceeds a value of about 300 (see Figure 4 of Antonia et al. [57]). This is in contrast to the significant amount of experimental support in the context of the  $Re_\lambda$  independence of  $S_{\partial u/\partial x}$  in various flows when  $Re_\lambda \gtrsim 300$ , as discussed in Section 2. We have already commented [57,58] on the behaviour of the Kolmogorov-normalized spectra and  $S_{\partial u/\partial x}$  for forced periodic box turbulence. Briefly, they are not consistent with the following:

- (i) the  $(u_\kappa, \eta)$  scaling, inferred from the N-S equation, e.g., [46] (see also Section 3.2);

- (ii) the support for the  $(u_K, \eta)$  scaling from earlier DNS studies in forced periodic box turbulence, e.g., [63,88–90], for  $Re_\lambda$  up to 700 (see for example the Figure 1 of Yeung et al. [90] which show that  $S_{\partial u/\partial x}$  is constant for  $Re_\lambda \approx 240$ –700);
- (iii) the overwhelming support for the  $(u_K, \eta)$  scaling from experimental and EDQNM data in various other flows, as reviewed in this paper.

Also, the scaling range exponent  $\zeta_2$  for  $\overline{(\delta u)^2}$  in forced periodic box turbulence is about 0.72 [91–93]. However, in the same flow, McComb et al. [94,95] found that  $\zeta_2$  decreases with increasing  $Re_\lambda$  and  $\zeta_2 \rightarrow 0.679$  as  $Re_\lambda \rightarrow \infty$ . This is consistent with the EDQNM results of Meldi et al. [31] which show that, when  $Re_\lambda = 10^6$ ,  $\zeta_2$  approaches a value of about 0.674 in the scaling range.

Finally, it is worth recalling that the intermittency of the velocity field, which is intrinsic to the N-S equations, is reflected in quantities such as  $S_{\partial u/\partial x}$  and the flatness of  $\partial u/\partial x$  ( $F_{\partial u/\partial x}$ ). For the flows considered in Antonia et al. [49], Djenidi et al. [53], Tang et al. [58], these quantities saturate beyond a certain value of  $Re_\lambda$ . Intermittency is also intrinsic to the heat transport equation. It is well known that the passive scalar field is more intermittent than the velocity field, e.g., [1,96]. Even so, the available DNS data for forced periodic box turbulence show that both the Kolmogorov–Batchelor-normalized scalar spectra in the dissipative range collapse reasonably well and the mixed velocity derivative–temperature derivative skewness is approximately constant when the Prandtl number is close to 1 [97]. Evidently, it is desirable to do a thorough review of the small-scale statistics in forced periodic box turbulence for velocity and passive scalar fields; this is beyond the scope of our review.

**Author Contributions:** Conceptualization, S.L.T. and R.A.A.; writing—original draft preparation, S.L.T., L.D. and R.A.A.; writing—review and editing, S.L.T., L.D. and R.A.A.; visualization, S.L.T. All authors have read and agreed to the published version of the manuscript.

**Funding:** This research was supported by the National Natural Science Foundation of China (project no. 91952109), Guangdong Basic and Applied Basic Research Foundation (project no. 2023B1515020069), Shenzhen Science and Technology Program (project nos. RYX2021070609204-6085 and GXWD20220817171516009) and Fundamental Research Funds for the Central Universities (project no. HIT.OCEF.2024016).

**Institutional Review Board Statement:** Not applicable.

**Informed Consent Statement:** Not applicable.

**Data Availability Statement:** Not applicable.

**Conflicts of Interest:** The authors declare no conflicts of interest.

## References

1. Sreenivasan, K.; Antonia, R.A. The phenomenology of small-scale turbulence. *Ann. Rev. Fluid Mech.* **1997**, *29*, 435–472. [[CrossRef](#)]
2. Qian, J. Inertial range and the finite Reynolds number effect of turbulence. *Phys. Rev. E* **1997**, *55*, 337–342. [[CrossRef](#)]
3. Qian, J. Slow decay of the finite Reynolds number effect of turbulence. *Phys. Rev. E* **1999**, *60*, 3409. [[CrossRef](#)] [[PubMed](#)]
4. Kármán, T.V.; Howarth, L. On the statistical theory of isotropic turbulence. *Proc. R. Soc. Lond. A* **1938**, *164*, 192–215. [[CrossRef](#)]
5. Danaila, L.; Anselmetti, F.; Zhou, T.; Antonia, R.A. A generalization of Yaglom’s equation which accounts for the large-scale forcing in heated decaying turbulence. *J. Fluid Mech.* **1999**, *391*, 359–372. [[CrossRef](#)]
6. Lin, C.C. *Remarks on the Spectrum of Turbulence Proc First Symposium of Applied Mathematics*; American Mathematical Society: Providence, RI, USA, 1947; pp. 81–86.
7. Kolmogorov, A.N. Dissipation of energy in the locally isotropic turbulence. *Proc. R. Soc. Lond. A* **1991**, *434*, 15–17.
8. McComb, W.D. *Homogeneous, Isotropic Turbulence, Phenomenology, Renormalization and Statistical Closures*; Oxford University Press: Oxford, UK, 2014.
9. Batchelor, G.K. Kolmogoroff’s theory of locally isotropic turbulence. *Proc. Camb. Phil. Soc.* **1947**, *43*, 533–559. [[CrossRef](#)]
10. Monin, A.S. The theory of locally isotropic turbulence. *Dokl. Akad. Nauk. SSSR* **1959**, *125*, 515–518.
11. Frisch, U. *Turbulence: The Legacy of AN Kolmogorov*; Cambridge University Press: Cambridge, UK, 1995.
12. Lindborg, E. A note on Kolmogorov’s third-order structure-function law, the local isotropy hypothesis and the pressure–velocity correlation. *J. Fluid Mech.* **1996**, *326*, 343–356. [[CrossRef](#)]
13. Hill, R.J. Applicability of Kolmogorov’s and Monin’s equations of turbulence. *J. Fluid Mech.* **1997**, *353*, 67–81. [[CrossRef](#)]

14. Monin, A.S.; Yaglom, A.M. *Statistical Fluid Dynamics*; MIT: Hongkong, 2007; Volume 2.
15. Yaglom, A.M. Modern state of Kolmogorov's theory of developed turbulence. In *Advances in Turbulence X*; Andersson, H.I., de Krogstad, P.Å., Eds.; CIMNE: Barcelona, Spain, 2004; pp. 443–448.
16. Kármán, T.V.; Lin, C.C. On the concept of similiarity in the theory of isotropic turbulence. *Rev. Modern Phys.* **1949**, *21*, 516–519. [[CrossRef](#)]
17. Kolmogorov, A.N. The local structure of turbulence in incompressible viscous fluid for very large Reynolds number. *Proc. R. Soc. Lond. A* **1991**, *434*, 9–13.
18. Qian, J. Normal and anomalous scaling of turbulence. *Phys. Rev. E* **1998**, *58*, 7325–7329. [[CrossRef](#)]
19. Lindborg, E. Correction to the four-fifths law due to variations of the dissipation. *Phys. Fluids* **1999**, *11*, 510. [[CrossRef](#)]
20. Moisy, F.; Tabeling, P.; Willaime, H. Kolmogorov equation in a fully developed turbulence experiment. *Phys. Rev. Lett.* **1999**, *82*, 3994–3997. [[CrossRef](#)]
21. Lundgren, T.S. Kolmogorov two-thirds law by matched asymptotic expansion. *Phys. Fluids* **2002**, *14*, 638–642. [[CrossRef](#)]
22. Lundgren, T.S. Kolmogorov turbulence by matched asymptotic expansions. *Phys. Fluids* **2003**, *15*, 1074–1081. [[CrossRef](#)]
23. Antonia, R.A.; Burattini, P. Approach to the 4/5 law in homogeneous isotropic turbulence. *J. Fluid Mech.* **2006**, *550*, 175–184. [[CrossRef](#)]
24. Tchoufag, J.; Sagaut, P.; Cambon, C. Spectral approach to finite Reynolds number effects on Kolmogorov's 4/5 law in isotropic turbulence. *Phys. Fluids* **2012**, *24*, 015107. [[CrossRef](#)]
25. Sagaut, P.; Cambon, C. *Homogeneous Turbulence Dynamics*; Springer: Berlin/Heidelberg, Germany, 2018.
26. Bos, W.J.T.; Chevillard, L.; Scott, J.F.; Rubinstein, R. Reynolds number effect on the velocity increment skewness in isotropic turbulence. *Phys. Fluids* **2012**, *24*, 015108. [[CrossRef](#)]
27. Ni, R.; Xia, K. Kolmogorov constants for the second-order structure function and the energy spectrum. *Phys. Rev. E* **2013**, *87*, 023002. [[CrossRef](#)] [[PubMed](#)]
28. Boschung, J.; Gauding, M.; Hennig, F.; Denker, D.; Pitsch, H. Finite Reynolds number corrections of the 4/5 law for decaying turbulence. *Phys. Rev. Fluids* **2016**, *1*, 064403. [[CrossRef](#)]
29. Tang, S.L.; Antonia, R.A.; Djenidi, L.; Danaïla, L.; Zhou, Y. Finite Reynolds number effect on the scaling range behavior of turbulent longitudinal velocity structure functions. *J. Fluid Mech.* **2017**, *820*, 341–369. [[CrossRef](#)]
30. Antonia, R.; Tang, S.; Djenidi, L.; Zhou, Y. Finite Reynolds number effect and the 4/5 law. *Phys. Rev. Fluids* **2019**, *4*, 084602. [[CrossRef](#)]
31. Meldi, M.; Djenidi, L.; Antonia, R.A. Sensitivity analysis of the second and third-order velocity structure functions to the Reynolds number in decaying and forced isotropic turbulence using the EDQNM model. *Eur. J. Mech.-B/Fluids* **2021**, *88*, 229–242. [[CrossRef](#)]
32. Tang, S.L.; Antonia, R.A.; Djenidi, L. Dual scaling and the  $n$ -thirds law in grid turbulence. *J. Fluid Mech.* **2023**, *975*, A32. [[CrossRef](#)]
33. Mydlarski, L.; Warhaft, Z. On the onset of high-Reynolds-number grid-generated wind tunnel turbulence. *J. Fluid Mech.* **1996**, *320*, 331–368. [[CrossRef](#)]
34. Mydlarski, L.; Warhaft, Z. Passive scalar statistics in high-Peclet-number grid turbulence. *J. Fluid Mech.* **1998**, *358*, 135–175. [[CrossRef](#)]
35. Gylfason, A.; Ayyalasomayajula, S.; Warhaft, Z. Intermittency, pressure and acceleration statistics from hot-wire measurements in wind-tunnel turbulence. *J. Fluid Mech.* **2004**, *501*, 213–229. [[CrossRef](#)]
36. Bodenschatz, E.; Bewley, G.; Nobach, H.; Sinhuber, M.; Xu, H. Variable density turbulence tunnel facility. *Rev. Sci. Instruments* **2014**, *85*, 093908. [[CrossRef](#)]
37. Sinhuber, M.; Bodenschatz, E.; Bewley, G.P. Decay of turbulence at high Reynolds numbers. *Phys. Rev. Lett.* **2015**, *114*, 034501. [[CrossRef](#)] [[PubMed](#)]
38. Sinhuber, M.; Bewley, G.P.; Bodenschatz, E. Dissipative effects on inertial-range statistics at high Reynolds numbers. *Phys. Rev. Lett.* **2017**, *119*, 134502. [[CrossRef](#)] [[PubMed](#)]
39. Kaminsky, J.; Birnir, B.; Bewley, G.P.; Sinhuber, M. Reynolds number dependence of the structure functions in homogeneous turbulence. *J. Nonlinear Sci.* **2020**, *30*, 1081–1114. [[CrossRef](#)]
40. Kuchler, C.; Bewley, G.P.; Bodenschatz, E. Universal Velocity Statistics in Decaying Turbulence. *Phys. Rev. Lett.* **2023**, *131*, 024001. [[CrossRef](#)] [[PubMed](#)]
41. Kolmogorov, A.N. A refinement of previous hypotheses concerning the local structure of turbulence in a viscous incompressible fluid at high Reynolds number. *J. Fluid Mech.* **1962**, *13*, 82–85. [[CrossRef](#)]
42. Oboukhov, A. Some specific features of atmospheric turbulence. *J. Fluid Mech.* **1962**, *13*, 77–81. [[CrossRef](#)]
43. Frisch, U.; Sulem, P.L.; Nelkin, M. A simple dynamical model of intermittent fully developed turbulence. *J. Fluid Mech.* **1978**, *87*, 719–736. [[CrossRef](#)]
44. She, Z.S.; Leveque, E. Universal scaling laws in fully developed turbulence. *Phys. Rev. Lett.* **1994**, *72*, 336. [[CrossRef](#)]
45. Maurer, J.; Tabeling, P.; Zocchi, G. Statistics of turbulence between two counterrotating disks in low-temperature helium gas. *EPL (Europhys. Lett.)* **1994**, *26*, 31. [[CrossRef](#)]
46. Antonia, R.A.; Djenidi, L.; Danaïla, L. Collapse of the turbulent dissipation range on Kolmogorov scales. *Phys. Fluids* **2014**, *26*, 045105. [[CrossRef](#)]
47. Tennekes, I.; Lumley, J. *A First Course in Turbulence*; MIT Press: Cambridge, MA, USA, 1972.

48. Gamard, S.; George, W.K. Reynolds number dependence of energy spectra in the overlap region of isotropic turbulence. *Flow Turbul. Combust.* **2000**, *63*, 443–477. [[CrossRef](#)]
49. Antonia, R.A.; Djenidi, L.; Danaïla, L.; Tang, S.L. Small scale turbulence and the finite Reynolds number effect. *Phys. Fluids* **2017**, *29*, 020715. [[CrossRef](#)]
50. Tang, S.L.; Antonia, R.A.; Djenidi, L.; Zhou, Y. Can small-scale turbulence approach a quasi-universal state? *Phys. Rev. Fluids* **2019**, *4*, 024607. [[CrossRef](#)]
51. Qian, J. Closure approach to high-order structure functions of turbulence. *Phys. Rev. Lett.* **2000**, *84*, 646. [[CrossRef](#)] [[PubMed](#)]
52. Shi, J.Z. Qian Jian (1939–2018) and his contribution to small-scale turbulence studies. *Phys. Fluids* **2021**, *33*, 041301. [[CrossRef](#)]
53. Djenidi, L.; Antonia, R.; Tang, S. Scale invariance in finite Reynolds number homogeneous isotropic turbulence. *J. Fluid Mech.* **2019**, *864*, 244–272. [[CrossRef](#)]
54. Dryden, H. A review of the statistical theory of turbulence. *Q. Appl. Maths* **1943**, *1*, 7–42. [[CrossRef](#)]
55. Batchelor, G. Energy decay and self-preserving correlation functions in isotropic turbulence. *Q. Appl. Math.* **1948**, *6*, 97–116. [[CrossRef](#)]
56. Meldi, M.; Sagaut, P. Further insights into self-similarity and self-preservation in freely decaying isotropic turbulence. *J. Turbul.* **2013**, *14*, 24–53. [[CrossRef](#)]
57. Antonia, R.A.; Tang, S.L.; Djenidi, L.; Danaïla, L. Boundedness of the velocity derivative skewness in various turbulent flows. *J. Fluid Mech.* **2015**, *781*, 727–744. [[CrossRef](#)]
58. Tang, S.L.; Antonia, R.A.; Djenidi, L.; Danaïla, L.; Zhou, Y. Reappraisal of the velocity derivative flatness factor in various turbulent flows. *J. Fluid Mech.* **2018**, *847*, 244–265. [[CrossRef](#)]
59. Bos, W.J.; Bertoglio, J.P. Lagrangian Markovianized field approximation for turbulence. *J. Turbul.* **2013**, *14*, 99–120. [[CrossRef](#)]
60. Comte-Bellot, G.; Corrsin, S. Simple Eulerian time correlation of full-and narrow-band velocity signals in grid-generated, ‘isotropic’ turbulence. *J. Fluid Mech.* **1971**, *48*, 273–337. [[CrossRef](#)]
61. Briard, A.; Gomez, T.; Cambon, C. Spectral modelling for passive scalar dynamics in homogeneous anisotropic turbulence. *J. Fluid Mech.* **2016**, *799*, 159–199. [[CrossRef](#)]
62. Saffman, P.G. Note on the decay of homogeneous turbulence. *Phys. Fluids* **1967**, *10*, 1349–1352. [[CrossRef](#)]
63. Gotoh, T.; Fukayama, D.; Nakano, T. Velocity field statistics in homogeneous steady turbulence obtained using a high-resolution direct numerical simulation. *Phys. Fluids* **2002**, *14*, 1065–1081. [[CrossRef](#)]
64. Gagne, Y.; Castaing, B.; Baudet, C.; Malecot, Y. Reynolds dependence of third-order velocity structure functions. *Phys. Fluids* **2004**, *16*, 482–485. [[CrossRef](#)]
65. Lesieur, M.; Schertzer, D. Amortissement autosimilaire d’une turbulence à grand nombre de Reynolds. *J. Mécanique* **1978**, *17*, 609–646.
66. Lesieur, M.; Ossia, S. 3D isotropic turbulence at very high Reynolds numbers: EDQNM study. *J. Turbul.* **2000**, *1*, N7. [[CrossRef](#)]
67. Davidson, P.A. The minimum energy decay rate in quasi-isotropic grid turbulence. *Phys. Fluids* **2011**, *23*, 085108. [[CrossRef](#)]
68. Loitsyansky, L. Some basic laws of isotropic turbulence. *Trudy Tsentr. Aero.-Gidrodin Inst.* **1939**, *440*, 3–23.
69. Hill, R.J. Equations relating structure functions of all orders. *J. Fluid Mech.* **2001**, *434*, 379–388. [[CrossRef](#)]
70. George, W.K. The self-preservation of turbulent flows and its relation to initial conditions and coherent structures. In *Advances in Turbulence*; Arndt, G., Eds.; Hemisphere: New York, NY, USA, 1989; pp. 39–73.
71. George, W.K. Some new ideas for similarity of turbulent shear flows. In *Proceedings of Turbulence Heat and Mass Transfer Symposium Lisbon, Portugal*; Pereira, H., Eds.; Begell House: New York, NY, USA, 1994; pp. 24–49.
72. Djenidi, L.; Antonia, R.A.; Tang, S.L. Scaling of turbulent velocity structure functions: plausibility constraints. *J. Fluid Mech.* **2023**, *965*, A14. [[CrossRef](#)]
73. Hill, R.J.; Wilczak, J.M. Pressure structure functions and spectra for locally isotropic turbulence. *J. Fluid Mech.* **1995**, *296*, 247–269. [[CrossRef](#)]
74. Meldi, M.; Sagaut, P. Pressure statistics in self-similar freely decaying isotropic turbulence. *J. Fluid Mech.* **2013**, *717*, R2. [[CrossRef](#)]
75. Tsuji, Y.; Ishihara, T. Similarity scaling of pressure fluctuation in turbulence. *Phys. Rev. E* **2003**, *68*, 026309. [[CrossRef](#)] [[PubMed](#)]
76. Peters, N.; Boschung, J.; Gauding, M.; Goebbert, J.H.; Hill, R.J.; Pitsch, H. Higher-order dissipation in the theory of homogeneous isotropic turbulence. *J. Fluid Mech.* **2016**, *803*, 250–274. [[CrossRef](#)]
77. Boschung, J.; Hennig, F.; Gauding, M.; Pitsch, H.; Peters, N. Generalised higher-order Kolmogorov scales. *J. Fluid Mech.* **2016**, *794*, 233–251. [[CrossRef](#)]
78. Boschung, J. Exact relations between the moments of dissipation and longitudinal velocity derivatives in turbulent flows. *Phys. Rev. E* **2015**, *92*, 043013. [[CrossRef](#)]
79. Gauding, M.; Danaïla, L.; Varea, E. High-order structure functions for passive scalar fed by a mean gradient. *Int. J. Heat Fluid Flow* **2017**, *67*, 86–93. [[CrossRef](#)]
80. Saddoughi, S.G.; Veeravalli, S.V. Local isotropy of turbulent boundary layers at high Reynolds number. *J. Fluid Mech.* **1994**, *268*, 333–372. [[CrossRef](#)]
81. Pope, S.B. *Turbulent Flows*; Cambridge University Press: Cambridge, UK, 2000.
82. Larssen, J.V.; Devenport, W.J. On the generation of large-scale homogeneous turbulence. *Exp. Fluids* **2011**, *50*, 1207–1223. [[CrossRef](#)]

83. Tang, S.L.; Antonia, R.A.; Djenidi, L.; Zhou, Y. Scaling of the turbulent energy dissipation correlation function. *J. Fluid Mech.* **2020**, *891*, A26. [[CrossRef](#)]
84. Ishihara, T.; Kaneda, Y.; Yokokawa, M.; Itakura, K.; Uno, A. Small-scale statistics in high-resolution direct numerical simulation of turbulence: Reynolds number dependence of one-point velocity gradient statistics. *J. Fluid Mech.* **2007**, *592*, 335–366. [[CrossRef](#)]
85. Gauding, M. Statistics and Scaling Laws of Turbulent Scalar Mixing at High Reynolds Numbers. Ph.D. Thesis, RWTH Aachen University, Aachen, Germany, 2014.
86. Khurshid, S.; Donzis, A.; Sreenivasan, K.R. Energy spectrum in the dissipation range. *Phys. Rev. Fluids* **2020**, *3*, 082601. [[CrossRef](#)]
87. Buaria, D.; Sreenivasan, K.R. Dissipation range of the energy spectrum in high Reynolds number turbulence. *Phys. Rev. Fluids* **2020**, *5*, 092601. [[CrossRef](#)]
88. Jimenez, J.; Wray, A.A.; Saffman, P.G.; Rogallo, R.S. The structure of intense vorticity in isotropic turbulence. *J. Fluid Mech.* **1993**, *255*, 65–90. [[CrossRef](#)]
89. Yeung, P.K.; Zhou, Y. Universality of the Kolmogorov constant in numerical simulations of turbulence. *Phys. Rev. E* **1997**, *56*, 1746–1752. [[CrossRef](#)]
90. Yeung, P.K.; Donzis, D.A.; Sreenivasan, K.R. High-Reynolds-number simulation of turbulent mixing. *Phys. Fluids* **2005**, *17*, 081703. [[CrossRef](#)]
91. Iyer, K.P.; Sreenivasan, K.R.; Yeung, P.K. Reynolds number scaling of velocity increments in isotropic turbulence. *Phys. Rev. E* **2017**, *95*, 021101. [[CrossRef](#)]
92. Iyer, K.P.; Sreenivasan, K.R.; Yeung, P.K. Scaling exponents saturate in three-dimensional isotropic turbulence. *Phys. Rev. Fluids* **2020**, *5*, 054605. [[CrossRef](#)]
93. Ishihara, T.; Kaneda, Y.; Morishita, K.; Yokokawa, M.; Uno, A. Second-order velocity structure functions in direct numerical simulations of turbulence with  $R_\lambda$  up to 2250. *Phys. Rev. Fluids* **2020**, *5*, 104608. [[CrossRef](#)]
94. McComb, W.D.; Yoffe, S.R.; Berera, A. A new method of identifying self-similarity in isotropic turbulence. *arXiv* **2013**, arXiv:1307.4575.
95. McComb, W.; Yoffe, S.; Linkmann, M.; Berera, A. Spectral analysis of structure functions and their scaling exponents in forced isotropic turbulence. *Phys. Rev. E* **2014**, *90*, 053010. [[CrossRef](#)]
96. Warhaft, Z. Passive scalars in turbulent flows. *Ann. Rev. Fluid Mech.* **2000**, *32*, 203–240. [[CrossRef](#)]
97. Tang, S.L.; Antonia, R.A.; Djenidi, L.; Danaila, L.; Zhou, Y. Boundedness of the mixed velocity-temperature derivative skewness in homogeneous isotropic turbulence. *Phys. Fluids* **2016**, *28*, 095102. [[CrossRef](#)]

**Disclaimer/Publisher’s Note:** The statements, opinions and data contained in all publications are solely those of the individual author(s) and contributor(s) and not of MDPI and/or the editor(s). MDPI and/or the editor(s) disclaim responsibility for any injury to people or property resulting from any ideas, methods, instructions or products referred to in the content.